

AD-A258 710



2

PL-TR-92-2223

**DEVELOPMENT AND USE OF DATA ANALYSIS  
PROCEDURES FOR THE CRRES PAYLOADS  
AFGL-701-2/DOSIMETER AND AFGL-701-4/FLUXMETER  
AND APPLICATION OF THE DATA ANALYSIS  
RESULTS TO IMPROVE THE STATIC AND DYNAMIC  
MODELS OF THE EARTH'S RADIATION BELTS**

Bronislaw K. Dichter  
Frederick A. Hanser

PANAMETRICS, INC.  
221 Crescent Street  
Waltham, MA 02154

DTIC  
ELECTE  
NOV 2 1992  
S C D

17 August 1992

Final Report

July 1987 - August 1992

Approved for Public Release; Distribution Unlimited



**PHILLIPS LABORATORY  
Directorate of Geophysics  
AIR FORCE MATERIEL COMMAND  
HANSCOM AIR FORCE BASE, MA 01731-5000**

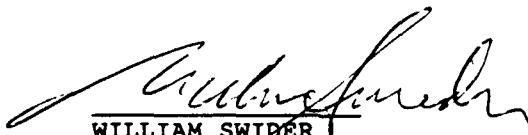
**92-29304**



"This technical report has been reviewed and is approved for publication"

  
MICHAEL D. VIOLET, LT, USAF  
Contract Manager

  
E. G. MULLEN  
Branch Chief

  
WILLIAM SWIDER  
Deputy Director

This document has been reviewed by the ESD Public Affairs Office (PA) and is releasable to the National Technical Information Service (NTIS).

Qualified requestors may obtain additional copies from the Defense Technical Information Center. All others should apply to the National Technical Information Service.

If your address has changed, or if you wish to be removed from the mailing list, or if the addressee is no longer employed by your organization, please notify PL/TSI, Hanscom AFB, MA 01731. This will assist us in maintaining a current mailing list.

Do not return copies of this report unless contractual obligations or notices on a specific document requires that it be returned.

REPORT DOCUMENTATION PAGE			Form Approved OMB No. 0704-0188	
<small>Public reporting burden for this collection of information is estimated to average 1 hour per response, including the time for reviewing instructions, searching existing data sources, gathering and maintaining the data needed, and completing and reviewing the collection of information. Send comments regarding this burden estimate or any other aspect of this collection of information, including suggestions for reducing this burden, to Washington Headquarters Services, Directorate for Information Operations and Reports, 1215 Jefferson Davis Highway, Suite 1204, Arlington, VA 22202-4302, and to the Office of Management and Budget, Paperwork Reduction Project (0704-0188), Washington, DC 20503.</small>				
1. AGENCY USE ONLY (Leave blank)		2. REPORT DATE 17 August 1992	3. REPORT TYPE AND DATES COVERED Final Report (July 1987 - August 1992)	
4. TITLE AND SUBTITLE Development and Use of Data Analysis Procedures for the CRRES Payloads AFGL-701-2/Dosimeter and AFGL-701-4/Fluxmeter and Application of the Data Analysis Results to Improve the Static & Dynamic Models of the Earth's Radiation Belts			5. FUNDING NUMBERS F19628-87-C-0169 PE 62101F PR 7601 TA 20 WU CF	
6. AUTHOR(S) Bronislaw K. Dichter Frederick A. Hanser			8. PERFORMING ORGANIZATION REPORT NUMBER	
7. PERFORMING ORGANIZATION NAME(S) AND ADDRESS(ES) PANAMETRICS, INC. 221 Crescent Street Waltham, MA 02154			10. SPONSORING / MONITORING AGENCY REPORT NUMBER PL-TR-92-2223	
9. SPONSORING / MONITORING AGENCY NAME(S) AND ADDRESS(ES) Phillips Laboratory Hanscom AFB, MA 01731-5000  Contracting Manager: Lt. Michael Violet/GPSP				
11. SUPPLEMENTARY NOTES				
12a. DISTRIBUTION / AVAILABILITY STATEMENT  Approved for public release; distribution unlimited.			12b. DISTRIBUTION CODE	
13. ABSTRACT (Maximum 200 words)  Response of the High Energy Electron Fluxmeter (instrument S/N 002) to electrons with energies between 1 and 4 MeV, as a function of instrument temperature, is described in this report.				
14. SUBJECT TERMS  Spacecraft Instrument, Electrons			15. NUMBER OF PAGES 28	
			16. PRICE CODE	
17. SECURITY CLASSIFICATION OF REPORT Unclassified	18. SECURITY CLASSIFICATION OF THIS PAGE Unclassified	19. SECURITY CLASSIFICATION OF ABSTRACT Unclassified	20. LIMITATION OF ABSTRACT SAR	

## Table of Contents

List of Figures . . . . .	iv
List of Tables . . . . .	iv
1. Introduction . . . . .	1
2. Experimental Work and Data Presentation . . . . .	2
2.1 Experimental Work . . . . .	2
2.2 Data Presentation . . . . .	3
2.2.1 Gain Shift . . . . .	3
2.2.2 Timing Distributions . . . . .	5
2.2.3 HEEF Electron Channel Count Rates . . . . .	9
3. HEEF Response Model . . . . .	12
4. Temperature Dependent Effective Geometric Factors . . . . .	18
5. Summary and Conclusions . . . . .	20
Appendix . . . . .	21
References . . . . .	23

DTIC QUALITY INSPECTED 4

Accession For	
NTIS GRA&I	<input checked="" type="checkbox"/>
DTIC TAB	<input type="checkbox"/>
Unannounced	<input type="checkbox"/>
Justification	
By	
Distribution/	
Availability Codes	
Avail and/or	
Dist	Special
A-1	

## List of Figures

<u>Figure</u>		<u>Page</u>
1	BGO-PMT system gain as a function of HEEF temperature. . . . .	4
2	SSDB-BGO timing signal delay as a function of temperature . . . . .	8
3	SSD-BGO timing distribution standard deviations as a function of electron energy deposited in the BGO . . . . .	10
4	Schematic timing pulse diagram . . . . .	13
5	Values of the error term calculated using eq. (3.8) . . . . .	16
6	Experimental and calculated normalized electron channel count rates . . . . .	17

## List of Tables

<u>Table</u>		<u>Page</u>
1	Summary of timing test results . . . . .	7
2	Normalized electron channel count rates . . . . .	11
A1	Coefficients for a polynomial fit to GF(E) . . . . .	21
A2	Parameters for eq. (A2) . . . . .	22

## 1. Introduction

The AFGL-701-4/Fluxmeter instrument (High Energy Electron Fluxmeter - HEEF S/N 0001) was launched aboard the CRRES spacecraft on July 25, 1990. The instrument was designed to measure electron flux in ten differential energy channels between 1 and 10 MeV. A full description of the instrument can be found in Ref. 1. It was intended that HEEF operate on-orbit at a temperature close to room temperature. However, due to thermal problems with another instrument in the same spacecraft compartment, the heaters in the compartment were turned off, and the operating HEEF temperature was, for most of the mission, between -10 and -12°C.

Questions arose about the performance of the HEEF instrument at the low temperatures, because of the known temperature dependence of the output signal of the BGO crystal, which formed the key detection element of the instrument. In order to determine the HEEF response, as a function of temperature, a series of experiments was carried out at Panametrics, Inc. in January and February of 1992 on the HEEF sister instrument (S/N 0002). This report contains a summary of the results of these experiments (Section 2), a simple mathematical model of the HEEF response (Section 3) and an outline of a method for correcting on-orbit HEEF data for instrument operating temperature (Section 4).

## 2. Experimental Work and Data Presentation

### 2.1 Experimental Work

Experimental work with HEEF (S/N 0002) was carried out both in a thermal vacuum chamber and in an environmental chamber under air pressure. Instrument response was measured at a variety of temperatures between +25°C and -15°C. In the vacuum chamber only electrons ( $^{106}\text{Ru}$  source) could be used to stimulate the instrument, while, in the environmental chamber, additional tests with pulsers were carried out in addition to the radioactive source work.

The  $^{106}\text{Ru}$  electron source produces electrons with energies up to 4 MeV, which covers about the half the HEEF energy range. In addition, the highest energy source electrons have sufficient energy to cause electron-positron pair creation in the HEEF casing material (predominantly tungsten). The subsequent annihilation of the positron results in the production of 511 keV  $\gamma$ -rays which can be detected in the BGO crystal. The 511 keV  $\gamma$ -ray peak was used to determine the gain change of the BGO-PMT system as a function of temperature as well as the absolute energy calibration of the BGO signal output.

The HEEF DPU output was recorded during the testing at each temperature to allow comparison of electron channel count rates at different temperatures. In addition, signals coming directly from the pre-amplifiers of the front and back solid state detectors (SSDF and SSDB) and the photomultiplier tube (PMT) viewing the scintillation light from the Bismuth Germanate (BGO) crystal were brought out from the instrument and connected to external electronic circuitry. This allowed energy and timing spectra of the various detectors to be measured and recorded independently of the HEEF DPU.

The position of the 511 keV peak in the BGO pulse height spectrum was measured at each temperature. The PMT high voltage setting was then changed, so that the 511 keV peak was in the same channel as it was at the temperature of +25°C. In this way, the pulse height spectrum from the BGO PMT was the same at all temperatures and the effects of gain shift, temperature and electron energy dependence of the triple coincidence efficiency could be measured separately and unambiguously.

The gain matching procedure was necessary because the energy spectrum of  $^{106}\text{Ru}$  electrons falls off steeply with increasing electron energy. Thus, an uncompensated gain shift would result in a different portion of the  $^{106}\text{Ru}$  electron spectrum contributing to a count rate in a given HEEF electron channel at different temperatures. In that case, an observed change in a channel count rate as a function of instrument temperature would be due to a complicated combination of gain shift and coincidence efficiency effects.

Once the gain of the BGO-PMT system was matched to the gain at  $+25^\circ\text{C}$ , a series of timing spectra were recorded. The SSDB signal was used to start a time-to-amplitude converter (TAC), while either the SSDF or the BGO signal was used to stop the conversion. The BGO signal was routed through a timing single channel analyzer so that only electrons with a narrow range of energy deposition in the BGO would give a valid TAC stop signal. In this way, the relative SSDB-BGO timing pulse distributions could be studied as a function of both temperature and incident electron energy.

## 2.2 Data Presentation

### 2.2.1 Gain Shift

The output of the PMT viewing the BGO crystal is temperature dependent. This dependence is a combination of two effects: 1) the decrease in gain of the PMT and 2) the increase in the BGO output signal with decreasing temperature. The net effect is a gain shift of the output of approximately  $-1\%/^\circ\text{C}$  (Ref. 2). The ratio of the centroid channel of the 511 keV  $\gamma$ -ray peak measured at a given temperature, to the centroid channel measured  $+25^\circ\text{C}$ , at a fixed PMT high voltage setting (HV Step = 200), is shown in Figure 1. The solid line is a linear fit to the data, and gives the gain shift as a function of instrument temperature,  $G_1(T)$ . The equation of the line is

$$G_1(T) = -6.328 \cdot 10^{-3} T + 1.183 \quad (2.1)$$

The gain also depends on the high voltage setting of the PMT ( $0 \leq \text{HV step} \leq 255$ ). As was discussed in Ref. 3, the gain shift as function of the HV step,  $G_2(\text{HV})$ , is given by



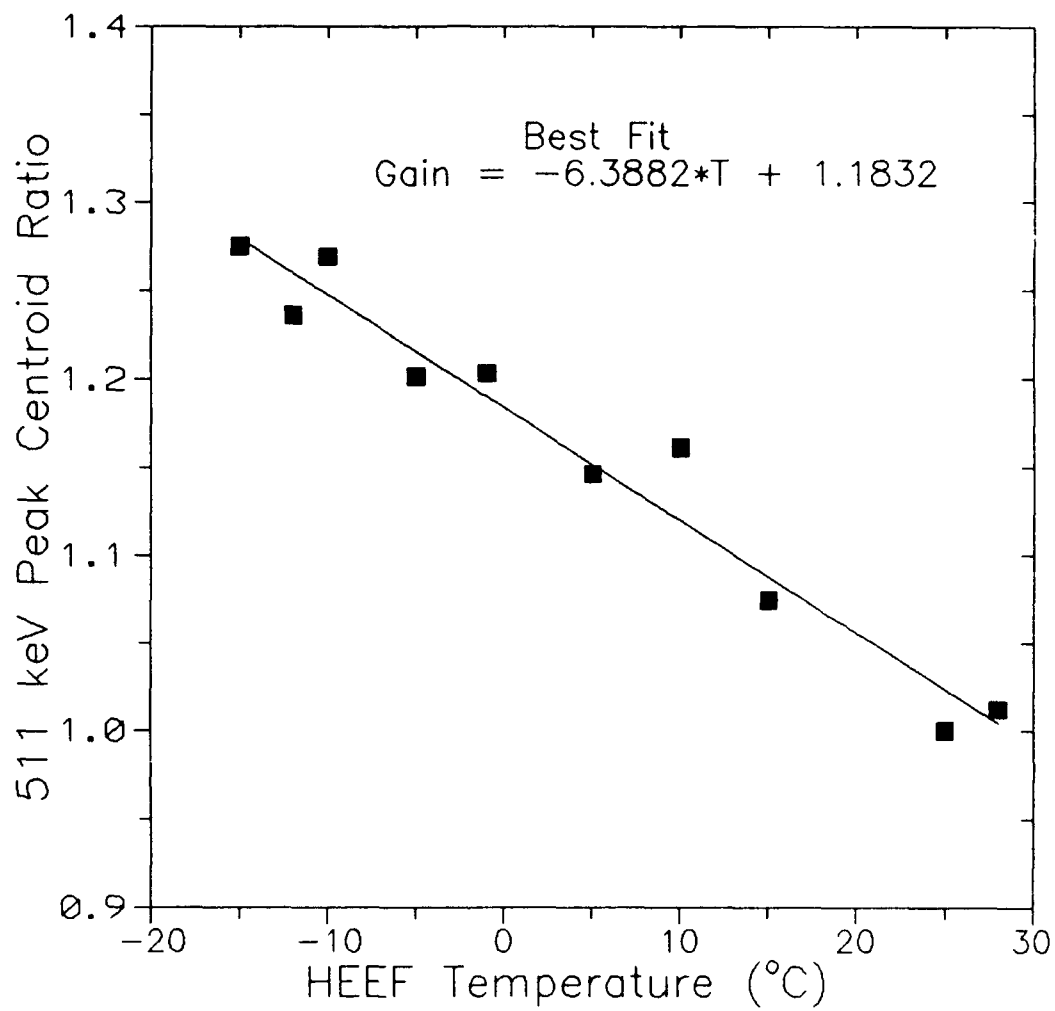


Figure 1. BGO-PMT system gain as function of HEEF temperature. Solid line is best linear fit to the data.

$$G_2(HV) = 3.438 \cdot 10^{-3} + 0.56 \quad (2.2)$$

The complete expression for the PMT-BGO gain shift is a product of  $G_1$  and  $G_2$

$$\begin{aligned} G(T, HV) &= G_1(T) \cdot G_2(HV) \\ &= -2.194 \cdot 10^{-5} HV \cdot T - 3.574 \cdot 10^{-3} T + \\ &\quad 4.068 \cdot 10^{-3} HV + 0.662 \end{aligned} \quad (2.3)$$

Equation 2.3 is slightly different from a similar equation, eq. (4.10), presented in Ref. 3. There are two reasons for the difference: 1) eq. (2.3) is referenced to the gain at +25°C while the equation in Ref. 3 was referenced to the gain at +20°C and 2) eq. (2.3) is based on a larger and more accurate data set than eq. (4.10). Despite the differences, the temperature dependent gains, calculated using the two equations, do not differ by more than a few tenths of one percent from each other.

Note that since the PMT-BGO gain depends on two independent parameters, high voltage and temperature, changes in one of the parameters can be used to offset changes in the other. This feature was used in the study of the timing distributions and channel count rates, described in the following two sections. At each temperature, the PMT high voltage setting was adjusted so that the 511 keV  $\gamma$ -ray peak centroid was in the same channel as at +25 °C. In this way, the temperature effects on the timing distributions and on the HEEF coincidence efficiency could be studied separately from the gain shift effects.

### 2.2.2 Timing Distributions

Study of the timing distributions showed that the relative timing of the SSDF and SSDB signals did not change with temperature or incident electron energy. This is to be expected because the SSDF and SSDB detectors are both similar Si solid state devices, and their electronic circuitry signal processing was essentially identical. The relative timing between the BGO and SSDF signals, on the other hand, showed a strong dependence on both instrument temperature and deposited energy.

The results obtained from the measured BGO-SSDB timing distributions, obtained in a thermal vacuum chamber using a  $^{106}\text{Ru}$  electron source, are listed in Table 1. The timing spectra were taken for different electron energy deposition ranges, each 600 keV broad.  $E_{\text{dep}}$  is the central energy of the electron energy deposition window. "All" signifies that all electron deposition energies were accepted for the timing spectrum. The third column label,  $\delta T$  is the difference between the times of arrival of the SSDB and BGO signals as measured by electronic circuitry external to HEEF. Note that, due to the artificial delays introduced in the external circuitry, the absolute value of  $\delta T$  is not meaningful; only differences between  $\delta T$  values have physical significance. The label on the last column,  $\sigma$  is the standard deviation of the BGO-SSDB timing distribution.

The  $\delta T$  values from Table 1 are shown plotted in Figure 2, together with a linear fit (solid line) of the  $\delta T$ -temperature relationship. It is evident that, as the temperature of the instrument decreases, the BGO timing signal delay relative to the SSDB timing signal increases. Superimposed on this large temperature effect, there is a smaller timing effect due to the magnitude of electron energy deposition.

The temperature effect on the BGO signal delay is due to the intrinsic properties of the scintillation light generation in the BGO crystal, and is not due to any electronic effects in HEEF. This was verified by measurements taken in air, in an environmental chamber, with both a  $^{106}\text{Ru}$  electron source and with a pulser. The  $^{106}\text{Ru}$  measurements, in air and at various temperatures, resulted in  $\delta T$  values identical, within the measurement accuracy, to those obtained in vacuum. This showed that there are no unexpected HEEF timing signal properties changes correlated with air pressure. The pulser signals, however, which were injected into the BGO and SSDB pre-amplifiers, showed no temperature effect at all. This indicates that the timing changes are inherent to the BGO crystal. This result is consistent with the well known fact that the BGO scintillation properties are highly temperature dependent (Ref. 2).

Table 1 Summary of Timing Test Results

Temp (°C)	E <sub>dep</sub> (MeV)	$\delta T$ (nsec)	$\sigma$ (nsec)
-15	All	372.6	44.5
-15	0.654	371.2	49.2
-15	0.938	375.5	42.9
-15	1.288	379.3	38.7
-15	1.607	380.2	34.5
-15	1.937	380.2	28.1
-15	2.256	379.9	31.5
-12	All	366.3	41.2
-12	0.654	363.9	45.9
-12	0.938	368.3	40.1
-12	1.288	371.5	36.5
-12	1.607	373.8	38.6
-12	1.937	373.6	31.8
-12	2.256	373.2	31.2
-5	All	354.1	35.5
-5	0.654	343.9	57.1
-5	0.938	349.4	45.3
-5	1.288	353.2	34.8
-5	1.607	355.0	36.4
-5	1.937	356.1	30.2
-5	2.256	355.5	27.8
+5	All	328.6	34.8
+5	0.654	321.0	34.9
+5	0.938	326.8	40.8
+5	1.937	334.7	26.9
+5	2.256	335.5	29.5
+15	All	301.6	33.1
+25	All	273.8	32.3
+25	0.654	266.8	40.6
+25	0.938	270.9	35.5
+25	1.288	274.9	30.6
+25	1.607	276.3	30.3
+25	1.937	277.2	28.5
+25	2.256	277.2	25.9
+25	2.575	277.5	25.9

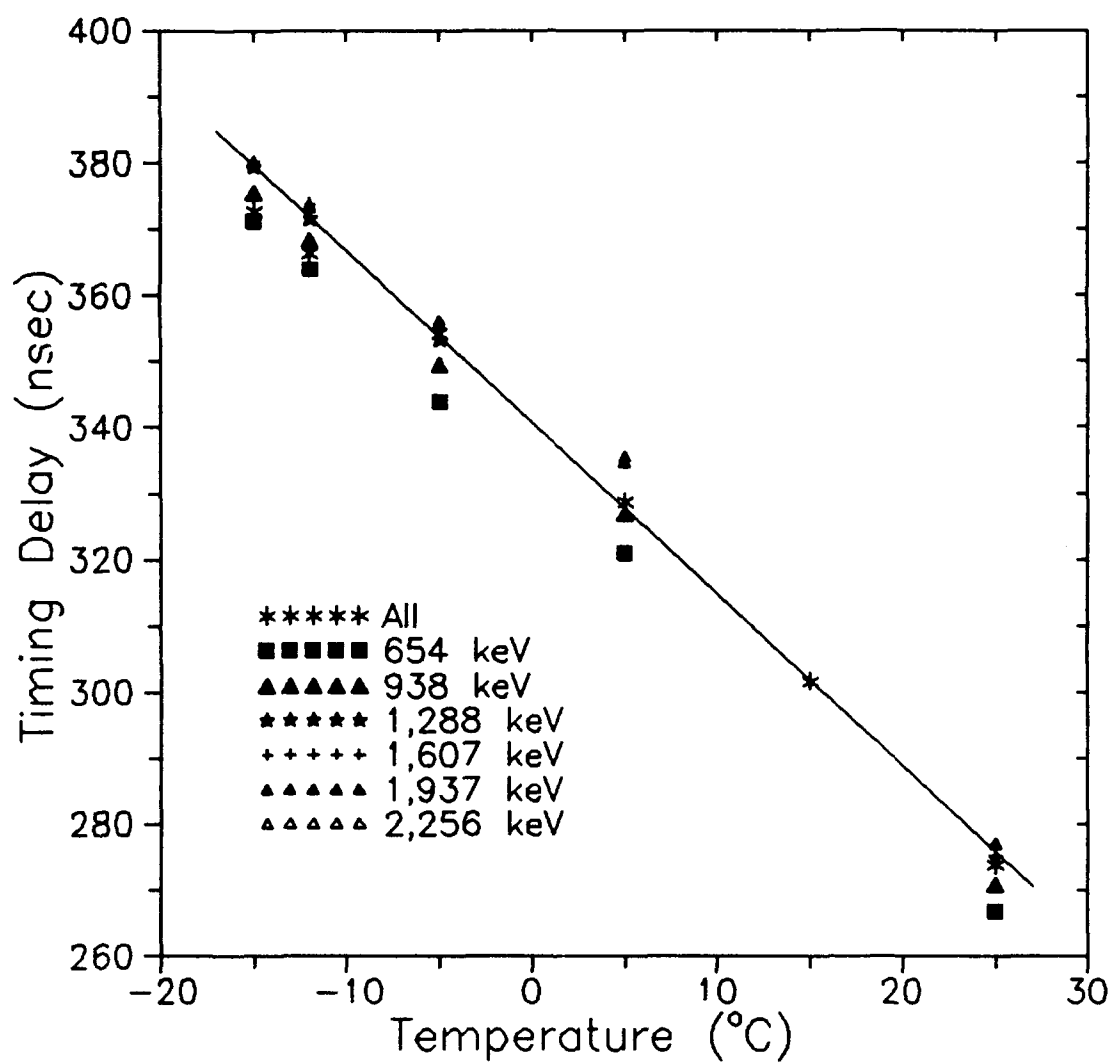


Figure 2. SSDB-BGO timing signal delay as a function of temperature. Only relative delay values have physical significance.

The width of the BGO-SSDB timing distributions also shows the effect of temperature and deposited energy. Shown plotted in Figure 3, are the standard deviations of the distributions at two temperatures (-15° and +25°C) as a function of deposited electron energy. Also shown are the fits to data of the form  $\sigma = A \cdot E_{\text{dep}}^B$ . Note that, as expected, the width of the timing distributions decreases as the signal magnitude increases. This is because the timing jitter, in the HEEF signal processing circuitry, has a larger effect on small amplitude signals than on the large amplitude ones. The temperature effect on  $\sigma$  is less significant than the  $E_{\text{dep}}$  effect.

### 2.2.3 HEEF Electron Channel Count Rates

The HEEF electron channel count rates (normalized to the count rates at +25 °C) as a function of HEEF temperature are listed in Table 2. The channel count rates at each temperature were obtained after the system gain was corrected for temperature effects, as described in Section 2.1. The  $^{106}\text{Ru}$  electron energy spectrum has an endpoint near 3.54 MeV so that the electron flux producing counts in L4-L5, and L5-L6 channels was low. In addition, because the electron spectrum is changing rapidly with energy near the endpoint, the channel count measurement is very sensitive to the HEEF gain correction. As a result, the data points at the highest measured energies have the largest uncertainties. The statistical (counting) uncertainty for the L5-L6 data is approximately 20% and the systematic uncertainty, due to errors in gain correction, is at least that large.

As can be seen from the data in Table 2, HEEF channel count rates decrease with decreasing temperature, although the decrease is not uniform with electron energy. The decrease in LL-L1 channel is about a factor of 4, going from +15 to -15°C, while the decrease in L5-L6 is nearly two orders of magnitude. A simple, one parameter, model of HEEF response as a function of temperature which can account for the observed count rates will be presented in Section 3.

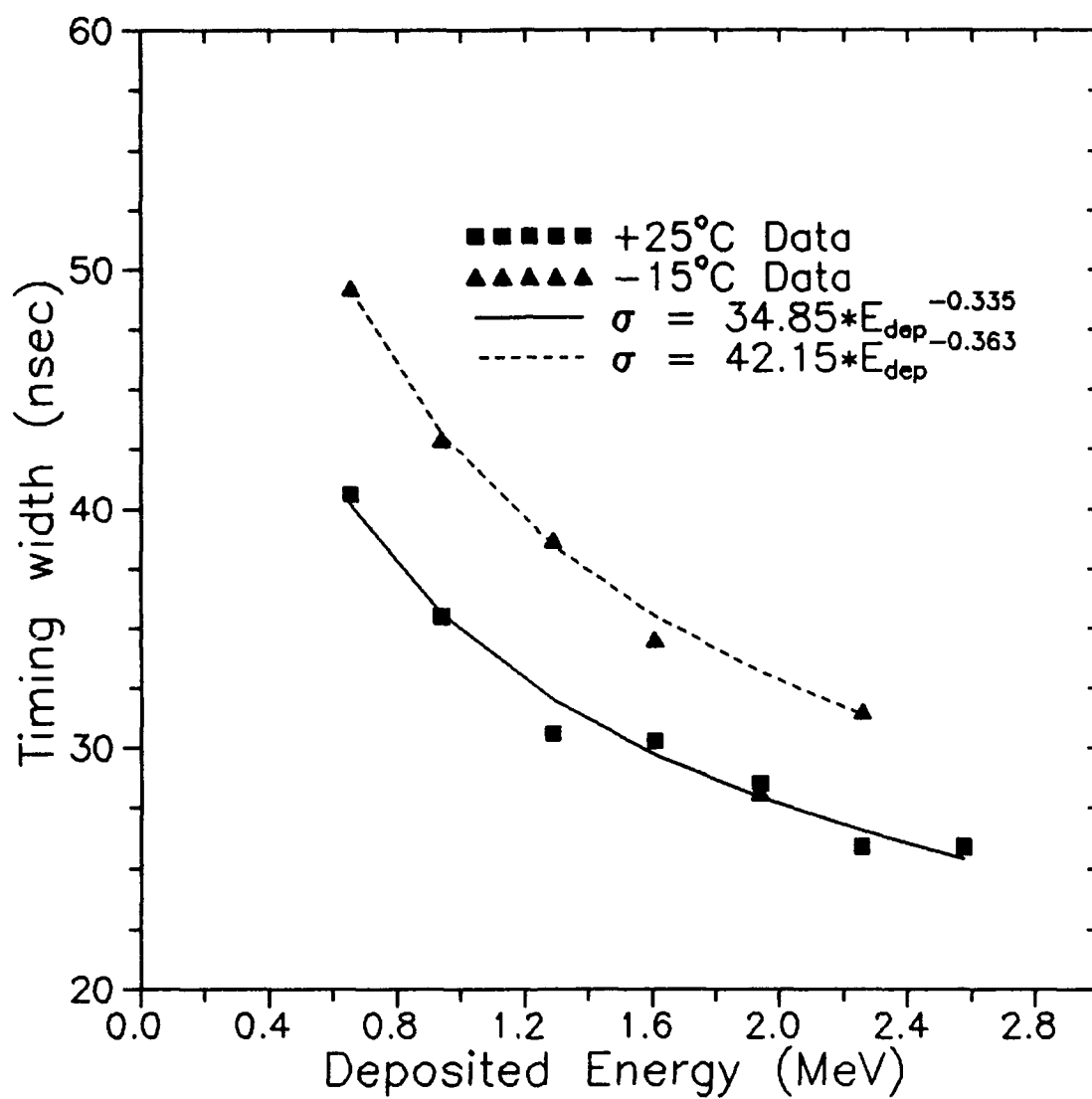


Figure 3. SSDB-BGO timing distribution standard deviations as a function of electron energy deposited in the BGO.

Table 2 Normalized Electron Channel Count Rates

Channel	Temperature (°C)				
	-15	-12	-5	+5	+15
L5-L6	0.020	0.069	0.188	0.820	1.880
L4-L5	0.035	0.078	0.239	0.695	1.286
L3-L4	0.055	0.088	0.249	0.668	1.124
L2-L3	0.067	0.101	0.251	0.631	1.006
L1-L2	0.104	0.137	0.286	0.573	0.957
LL-L1	0.191	0.226	0.375	0.562	0.915



### 3. HEEF Response Model

A triple coincidence (electron) count is recorded by HEEF when SSDF, SSDB and BGO signals arrive simultaneously at the coincidence gate. A simplified timing diagram is shown in Figure 4. Only one SSD timing pulse needs to be considered because the SSDF and SSDB pulse timing does not vary with either electron energy or temperature. Therefore, any timing offset or timing jitter between the SSDF and SSDB pulses will reduce the triple coincidence efficiency by a constant factor, regardless of temperature, and this effect is already included in the measured +25°C effective geometric factors.

In Figure 4, the SSD timing pulse arrives at  $t = 0$  and the BGO pulse after a time  $t_r + d(\theta)$ , where  $t_r$  is the SSD-BGO timing offset at +25°C and  $d(\theta)$  is an additional timing shift as a function of temperature,  $\theta$ . As drawn, both  $t_r$  and  $d(\theta)$  are both positive but in the model both positive and negative values of these quantities are allowed. If the overlap time of the two pulses ( $t_w$ ) is greater than 20 nsec a valid coincidence signal will result. Since the timing pulse duration is 86 nsec, the maximum possible time difference which can still give rise to a coincidence signal,  $d_m$ , is 66 nsec. The actual time difference between SSD and BGO signals, at a given temperature  $\theta$ , is not simply  $t_r + d(\theta)$  but is given by a distribution of values centered on  $t_r + d(\theta)$  with a standard deviation  $\sigma$ .

Given the model described above, the triple coincidence efficiency, as a function of incident electron energy ( $E$ ) and instrument temperature ( $\theta$ ),  $P(E, \theta)$  is given by

$$P(E, \theta) = \frac{1}{\sqrt{2} \sigma(E, \theta)} \int_{-d_m}^{d_m} \exp \left\{ \frac{-[t_r + d(\theta) - t]^2}{2 \cdot \sigma^2(E, \theta)} \right\} dt \quad (3.1)$$

Using a simple change of variables

$$y = \frac{[t_r + d(\theta) - t]}{\sqrt{2} \cdot \sigma(E, \theta)} \quad (3.2)$$

eq. (3.1) can be converted to

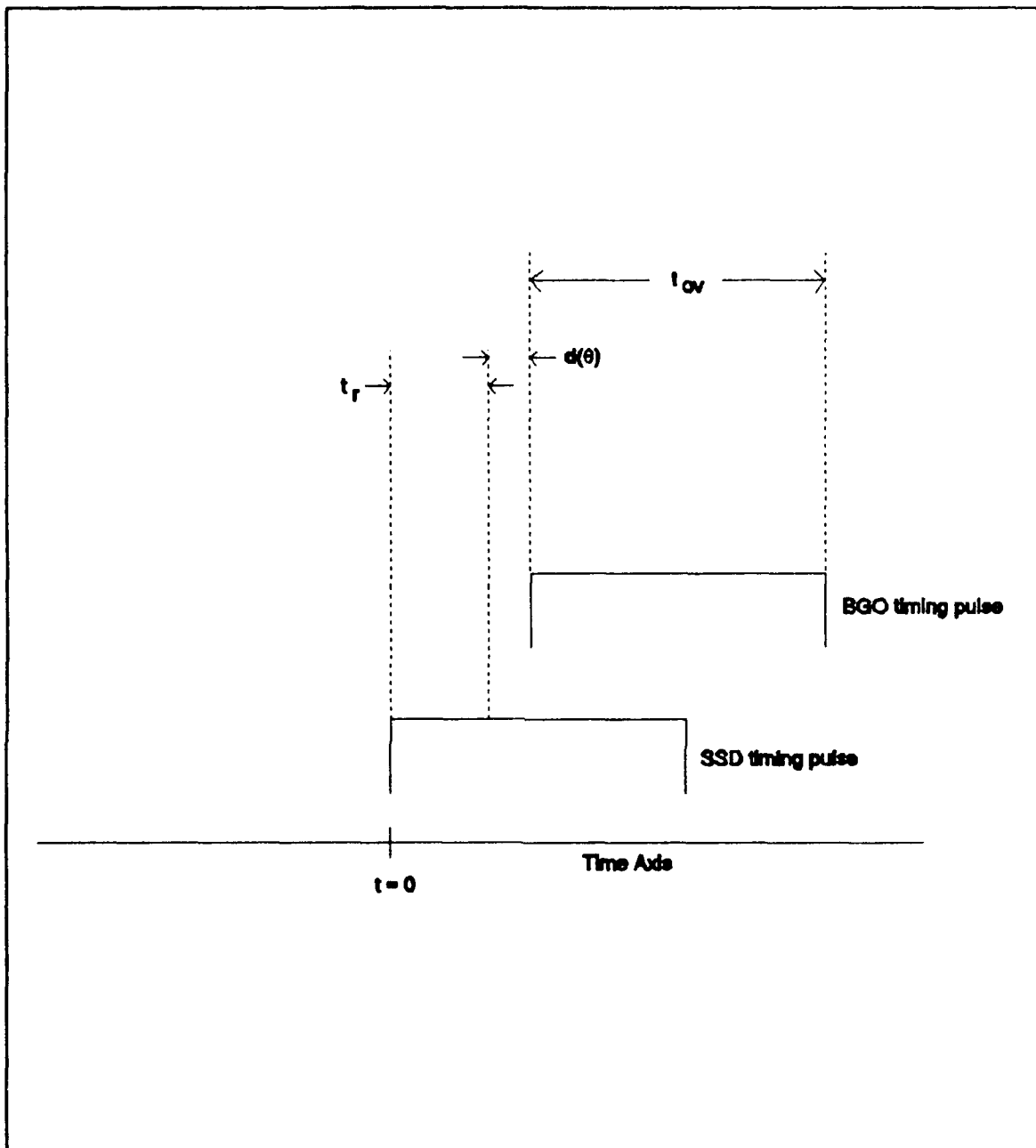


Figure 4. Schematic timing pulse diagram.

$$P(E, \theta) = \frac{1}{\sqrt{\pi}} \int_{D_-}^{D_+} \exp(-y^2) dy \quad (3.3)$$

where

$$D_{\pm}(E, \theta) = \frac{t_r + d(\theta) \pm d_m}{\sqrt{2} \cdot \sigma(E, \theta)} \quad (3.4)$$

The convenience of eq. (3.3) is that it can be evaluated in terms of the error function (erf) of the arguments  $D_{\pm}$ .

The model of the HEEF triple coincidence efficiency has only one adjustable parameter,  $t_r$ , the timing offset at  $+25^\circ\text{C}$ . All the other terms needed to evaluate eq. (3.1) can be derived from the data presented in Section 2.2.2. The timing signal shift, relative to the shift at  $+25^\circ\text{C}$ ,  $d(\theta)$ , is derived from the linear fit to the data from Table 1

$$d(\theta) = -2.5695 \cdot \theta + 64.2375 \text{ nsec} \quad (3.5)$$

The width of the timing distributions,  $\sigma$ , did not vary significantly with temperature and it was set to

$$\begin{aligned} \sigma(E, \theta) &= 34.855(E - 0.5)^{-0.3350} & \text{if } \theta \geq +5^\circ\text{C} \\ &= 42.155(E - 0.5)^{-0.3629} & \text{if } \theta < +5^\circ\text{C} \end{aligned} \quad (3.6)$$

Finally,  $d_m$  is known, from measurements taken with HEEF, to be 66 nsec.

In this model, the data of Table 2, are approximately given by

$$RC(E, \theta) = \frac{P(E, \theta)}{P(E, \theta = +25^\circ\text{C})} \quad (3.7)$$

where  $RC(E, \theta)$  are the normalized count rates. Equation 3.7 was evaluated, for various values of  $t_r$ , to find a best fit to the data. The fitting procedure minimized an error term,  $\epsilon$ , which was given by

$$\epsilon = \sum_i \sqrt{(RC_i^{calc} - RC_i^{meas})^2} \quad (3.8)$$

where  $RC_i^{meas}$  are the data points from Table 2 (plotted at the central channel energy) and  $RC_i^{calc}$  are the values calculated using eq. (3.7). A plot of the error term, as a function of the timing offset  $t_r$ , is shown in Figure 5. The minimum of  $\epsilon$  occurs at  $t_r = 13.5$  nsec, a physically reasonable value, given the uncertainties of adjusting the HEEF timing electronics.

The measured data points (Table 2) and curves calculated using eq. (3.7), with  $t_r = 13.5$  nsec, are shown in Figure 6. The agreement with the data is very good, except perhaps at the highest energy where the experimental uncertainties are the largest. A decrease in value of  $t_r$  beyond 5 nsec leads to calculated curves which are too flat (change too little with electron energy) to fit the data. On the other hand, a value of  $t_r$  larger than 20 nsec leads to curves which fall too steeply with increasing electron energy.

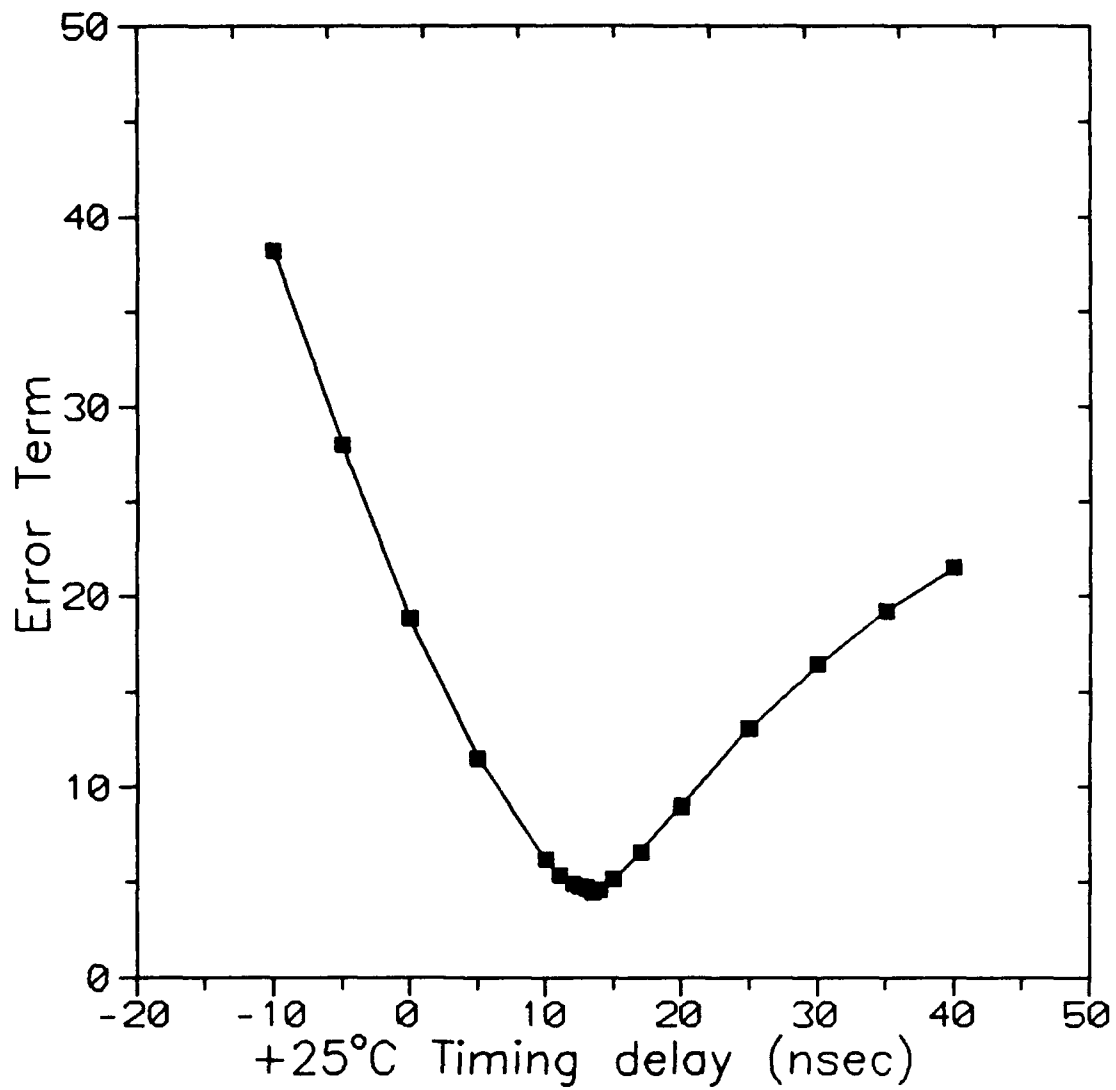


Figure 5. Values of the error term calculated using eq. (3.8). Solid line is drawn to guide the eye.

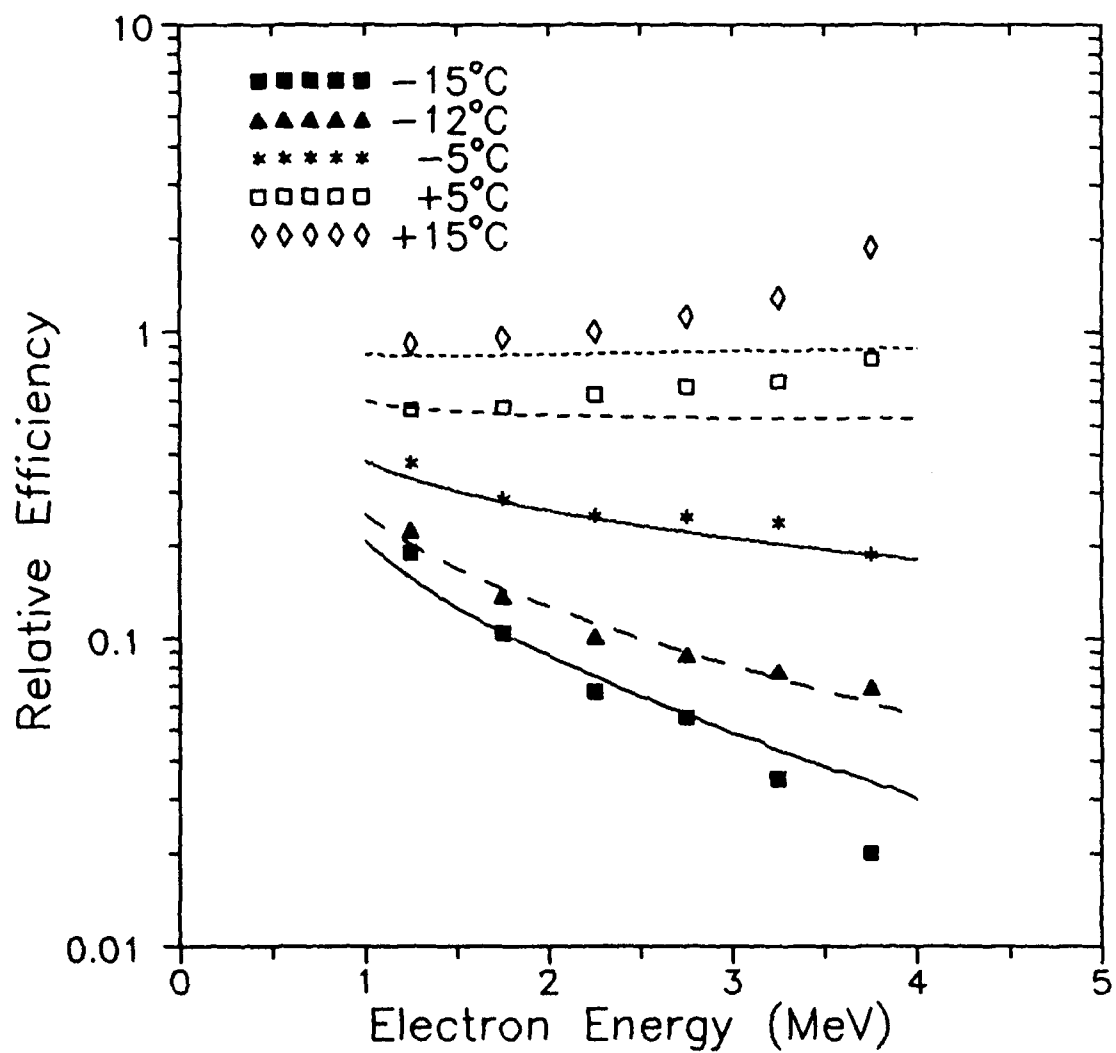


Figure 6. Experimental and calculated normalized electron channel count rates. Measured values are plotted as data points, lines are values calculated using eq. (3.7).

#### 4. Temperature Dependent Effective Geometric Factors

The effective geometric factors,  $G_n$ , for each of the ten HEEF electron channels ( $n=1$  for LL-L1,  $n=2$  for L1-L2 ...  $n=10$  for L9-L10) can be written down as a function of the PMT high voltage setting, the instrument temperature and the room temperature timing offset,  $t_r$ . The high voltage setting affects the BGO-PMT system gain, the temperature affects the gain and triple coincidence efficiency and the timing offset affects the triple coincidence efficiency. The factors  $G_n$  can be calculated from

$$G_n(T, HV) = \int_0^\infty GF(E) \cdot R_n(E, T, HV) \cdot P(E, T, t_r) dE \quad (4.1)$$

where  $GF$  is the energy dependent HEEF geometric factor,  $R_n$  is the channel response function and  $P$  is the triple coincidence efficiency.  $GF$  and  $R_n$  are given in the Appendix and  $P$  is given by eq. (3.1).

For the flight instrument (S/N 0001), the only unknown in eq. (4.1) is the timing offset,  $t_r$ . Although analysis of the instrument shows that this value is within 20 ns of zero, it is not possible to narrow the range any further with available calibration and test data. It is possible, however, to obtain a good estimate of this value by using on-orbit data.

Panametrics personnel performed an analysis of outer belt electron data from CRRES orbit 6 for both HEEF and the AFGL-701-2/Dosimeter electron channels. At that time, shortly after launch, HEEF was near room temperature. The analysis consisted of forming an incident electron spectrum using HEEF data, predicting the response of the Dosimeter electron channels to that spectrum, and comparing the predictions to the actual measured Dosimeter response. The agreement between the two instruments was very good. This indicates that the room temperature behavior of HEEF is well understood and that, when electron fluxes are not extreme, the output of the two instruments can be usefully compared to each other.

The value of  $t_r$  for the flight instrument can be extracted from on-orbit data by comparing the measured and predicted Dosimeter electron channel response, with the predicted response calculated from HEEF electron channel data with various values of  $t_r$ . This can be done for orbits after HEEF reached its final temperature of -10

to  $-12^{\circ}\text{C}$  and for orbits at an earlier time when the instrument was at temperatures intermediate between launch temperature and its final temperature. It is expected that the agreement between the Dosimeter and HEEF data will be maximized if the value of  $t_r$  used in the calculation will be within a few nsec of the true value. Once  $t_r$  is determined, all on-orbit HEEF data can be corrected for temperature effects and used in radiation belt modeling.



## 5. Summary and Conclusions

In response to questions that were raised about the validity of the calibration of the HEEF (S/N 0001) instrument, in view of the unexpectedly low operating on-orbit temperatures, a series of measurements on the sister instrument (S/N 0002) was carried out. The measurements were designed to measure instrument performance as a function of temperature.

Analysis of the results showed that the detection efficiency of the instrument for electrons decreases with temperature. This effect is due to a temperature dependence of the time of arrival of the BGO timing signal at the SSDF-SSDB-BGO coincidence gate. The timing shift was shown to be caused by the scintillation properties of the BGO crystal itself, rather than by any temperature dependence of the electronic signal processing circuitry. This is significant because the change in timing properties of the on-orbit unit (S/N 0001) will then be the same as the tested unit (S/N 0002).

A simple one parameter model of HEEF response to electrons was found to reproduce the experimental temperature data. The model parameter is the room temperature (+25°C) timing offset between the BGO and the SSDB timing signals,  $t_r$ . This offset is set during the testing and calibration process, by adjusting the relative timing of the BGO, SSDF and SSDB signals until the triple coincidence efficiency reaches maximum efficiency for detection of electrons. The accuracy of this procedure is of the order of 10-20 nsec, and the calculated value of  $t_r$ , 13.5 nsec (for HEEF Serial No. 0002), is consistent with this value. The HEEF response model allows the calculation of temperature dependent effective geometric factors for each of the HEEF electron channels once the parameter  $t_r$  is determined.

The value of  $t_r$  measured for HEEF Serial No. 0002 can not be directly transferred to the on-orbit unit. The accuracy of the procedure to set  $t_r$  during instrument calibration allows the value to  $t_r$  for S/N 0001 to be within 20 nsec on either side of zero. It should be possible, however, to deduce the value of the S/N 0001 timing offset from on-orbit data, by comparing HEEF and AFGL-701-2/Dosimeter data, and, therefore, to calculate the temperature corrections to be used for analysis of on-orbit HEEF data.

## Appendix

The energy dependent HEEF effective geometric factor,  $GF(E)$ , can be fit by ninth order polynomial (Ref. 3)

$$GF(E) = \sum_{i=0}^9 C_i \cdot E^i \quad (A.1)$$

with  $GF(E) = 0$  for  $E < 1$  MeV and  $GF(E) = GF(10 \text{ MeV})$  for  $E > 10$  MeV. The values of the coefficients  $C_i$  are listed in Table A1 below.

Table A1 Coefficients for a polynomial fit to $GF(E)$ . $GF(E) = \sum C_i \cdot E^i$	
i	$C_i$
0	0.00229551
1	-0.007063260
2	0.00740881
3	-0.003476120
4	0.00103210
5	-0.000205743
6	$2.70496 \cdot 10^{-5}$
7	$-2.22341 \cdot 10^{-6}$
8	$1.02801 \cdot 10^{-7}$
9	$-2.03266 \cdot 10^{-9}$

The channel response functions,  $R(E, L_n)$ , can be approximated by (Ref. 3)

$$R(E, L_n) = \begin{cases} M_n \exp(-(E-P_n^-)^2/2\sigma^2) & \text{if } E < P_n^- \\ M_n & \text{if } P_n^- \leq E \leq P_n^+ \\ M_n \exp(-(E-P_n^+)^2/2\sigma^2) & \text{if } E > P_n^+ \end{cases} \quad (\text{A.2})$$

where  $P_n^\pm = P_n \pm \delta P_n$ . The physical significance of the parameters in eq. (A.2) is as follows:  $P_n$  is the central energy of the channel,  $M_n$  is the relative channel geometric factor at  $E = P_n$ ,  $\delta P_n$  is the half width over which  $R(E, L_n) = M_n$  and  $\sigma_n$  is the edge falloff width. Values of the parameters in eq. (A.2) are listed below in Table A2.

Table A2 Parameters for eq. (A2)				
Channel	$M_n$	$P_n$ (MeV)	$\delta P_n$ (MeV)	$\sigma_n$ (MeV)
LL-L1	0.919	1.30	0.00	0.234
L1-L2	0.914	1.82	0.00	0.234
L2-L3	0.925	2.35	0.00	0.234
L3-L4	0.896	2.80	0.00	0.221
L4-L5	0.886	3.30	0.00	0.234
L5-L6	0.905	3.80	0.00	0.221
L6-L7	0.997	4.55	0.15	0.293
L7-L8	0.997	5.55	0.15	0.340
L9-L9	1.000	7.08	0.58	0.357
L9-L10	1.000	9.05	0.50	0.425

## References

1. J. L. Hunerwadel, B. Sellers and F. A. Hanser, "Design, Fabricate, Test and Deliver Two Satellite Electron Flux Detectors," Report AFGL-TR-87-0205 (June 1987), ADA190799.
2. C. L. Melcher, J. S. Schweitzer, L. . Lieberman and J. Simonetti, " Temperature Dependence of Fluorescence Decay time and Emission spectrum of Bismuth Germanate," IEEE Trans. Nucl. Sci. Vol. NS-32, p. 529-532 (1985).
3. B. K. Dichter and F. A. Hanser, "Development of the Use and Data Analysis Procedures for the CRRES Payloads AFGL-701-2/Dosimeter and AFGL-701-4/Fluxmeter and Application of the Data Analysis Results to Improve the Static and Dynamic Models of the Earth's Radiation Belts," Report PL-TR-91-2186 (July 1991), ADA241399.